UNCERTAINTY MODELING AND ANALYSIS OF SPACEBORNE INFRARED HYPERSPECTRAL IMAGES OVER RUGGED LAND SURFACE

Qiu, X.[1], Li, Z.[1], Liu, S.[1], Liu, T.[1], Jia, G.[2]

[1] Institute of Remote Sensing Satellite, China Academy of Space Technology, Beijing 100094, China - kathyq517@163.com
[2] School of Instrumentation and Optoelectronic Engineering, Beihang University, Beijing 100191, China - jiaguorui@buaa.edu.cn

KEY WORDS: Uncertainty Transfer, Hyperspectral Image, Land Surface Temperature, Rugged Land Surface, Modeling.

ABSTRACT: Infrared hyperspectral imaging is an important technical means to obtain the emissivity spectra and temperature of land surface target, and is an important development direction of spaceborne optical remote sensing in the future. Under the natural rugged land surface condition, the quality of infrared hyperspectral imaging data is affected by terrain condition, atmospheric condition and instrument performance. Therefore, the instrument signal-to-noise ratio and the calibration accuracy could not directly describe the measurement accuracy of the hyperspectral characteristics of target. An uncertainty prediction model of spaceborne infrared hyperspectral images over rugged land surface is established, in this paper. This model could simulate the surface scene, the atmospheric radiation transfer over rugged land surface, and the imaging process of the spaceborne spectrometer. At the same time, the uncertainty transfer from the surface signal to the restored radiance data product could be realized. The generated uncertainty results include the fluctuation of the surface signal, the error of the atmospheric transmission model, the influence of topographic relief, the response characteristics of the imaging spectrometer and the calibration uncertainty. Based on this model, we can also realize the ranking of the uncertainty contribution of the above links, which could help to identify the weak link in the remote sensing measurement chain. The random simulation experiments over a rugged desert scene were conducted to verified the model. It is indicated that more than 99.9% of the stochastic simulation radiance spectra are in the range of the predicted uncertainty.

1. INTRODUCTION

Infrared hyperspectral imaging technology could help to capture the spatial-spectral variations of land surface and atmosphere radiations, as well as to obtain the diagnostic features of ground objects (Tang, 2014). It has essential research value and application prospect. The imaging performance of airborne infrared hyperspectral imager has been continuously improved. The noise equivalent temperature difference of infrared hyperspectral instruments such as the HyTES (Johnson, 2011), ATHIS (Yuan, 2019) has reached about 0.2K. However, there are no earth observation satellite could provide mid and long wave infrared hyperspectral images, at present. The available infrared hyperspectral data is seriously insufficient. It is urgent to develop the spaceborne infrared hyperspectral imaging systems with high spatial resolution.

In the early stage to design spaceborne infrared hyperspectral imaging system, the imaging chain simulation is of great significance (Schott, 2007). The simulation tools such as the Digital Image and Remote Sensing Image Generation (Goodenough, 2017), the EnMAP End-to-End Simulation Tool (Cota, 2011), and the Parameterized Image Chain Analysis & Simulation Software (Segl, 2012), could predict the imaging signal under the formulated system parameters. Then the simulated images could be used to describe the performance of satellites. These simulation tools have been used in the design and optimization of spaceborne remote sensing systems such as the sentinel satellites and the EnMap satellite, were conducted.

Notably, the application of hyperspectral imaging satellites relies on the quantitative measurements, which is different from conventional optical remote sensing satellites. In the design and development stage of imaging spectrometer, the instrument designers generally provide the expected signal-to-noise ratio, the noise equivalent temperature difference, or the radiometric calibration accuracy to qualitatively describe the uncertainty of the spectrometer. However, the users of infrared hyperspectral systems are concerned about the uncertainty of data products such as the restored radiance, the land surface temperature and the land surface emissivity. The illumination condition over the rugged land surface, the radiation coupling between the atmosphere and land surface, the system noise, the system noise, the calibration uncertainty, as well as the errors of radiation model contribute to the measurement uncertainty of the infrared hyperspectral images. While the traditional image simulation tools could only provide the predicting results of the determinate imaging signal but not uncertainty.

In order to quantitatively predict the observed signal and measurement accuracy of the infrared hyperspectral system, it is necessary to simulate the scene, the atmospheric radiation transfer, and the imaging process, according to accurate infrared models. There are still some problems, including (1) current models could not describe the spatial-spectral signal over rugged and heterogeneous surface in the infrared spectral domain; (2) the measurement accuracy of surface signals could not be quantitatively described and predicted, due to the lack of uncertainty transfer model for the remote sensing process.

To fix the long-term neglect of atmosphere and terrain coupling radiation in the infrared imaging simulation chain, we have already established a model to simulate the remote sensing imaging signal over rugged and heterogeneous land surface (Qiu, 2022). Three convolution functions determined by topographic and atmospheric parameters were designed to quantify the relations among the direct ground leaving radiation with the topographic illumination effect, the trapping effect and the atmospheric adjacency effect. And the correlation between atmospheric and topographic effects was described analytically. As a result, the accurate modeling of the atmosphere and terrain coupling radiation was realized.

Based on our previous work of hyperspectral image simulation, this paper focuses on the uncertainty transfer model of the forward measurement process of infrared remote sensing. In the

forward simulation model, the uncertainty comes from the fluctuation of surface target characteristics, the uncertainty of atmospheric and topographic factors, the noise of imaging spectrometer, and the uncertainty of calibration and so on. In this paper, firstly, the influencing factors of uncertainty in the forward simulation model are traced and modeled. The uncertainty corresponding to DN image and restored radiance image is obtained pixel by pixel. Then the contribution factors of uncertainty are sorted, in order to provide reference for the integrated construction of infrared hyperspectral remote sensing satellite-ground processing system.

2. UNCERTAINTY MODELING METHODS

The uncertainty evaluation methods of remote sensing data products could be systematically divided into two ways: the posteriori way and the priori way. The posteriori method obtains the optimal estimation and the probability distribution of remote sensing observations by using statistical methods. The posteriori method has been widely used in the comparison and verifications of remote sensing products. The prior method needs to build the uncertainty transfer model, so as to estimate the uncertainty introduced by each link of the remote sensing process and each input parameter. Using a continuous transfer link of the measurement process, the prior method could realize the traceability of the measurement uncertainty, and has a guiding role for the determination of the optimal measurement scheme for a particular remote sensing system. Therefore, it is of great significance for the design of the application-oriented remote sensing system to describe remote sensing process and analyze the uncertainty of remote sensing products from the perspective of quantitatively traceability.

For the measurement process of different disciplines, the theory of uncertainty evaluation is similar. The Guide to the expression of uncertainty in measurement (GUM) provides a basic method for evaluating the measurement uncertainty (BIPM, 2008). For the uncertainty of the observed quantity that could be expressed analytically, the uncertainty of the measurement link could be synthesized by the formula method. For complex variables or processing processes that are difficult to be expressed analytically, Monte Carlo method could be used to carry out simulation experiments, Then, the distribution function and uncertainty of the random variables are obtained statistically using experimental results.

The implementation steps of uncertainty evaluation include: (1) the sources of measurement uncertainty are analyzed, and the significant uncertainty components are identified; (2) the standard uncertainty and degree of freedom of each component are evaluated respectively; (3) the covariances and correlations between each two uncertainty components are evaluated; (4) according to the measurement equation, the standard uncertainty is synthesized, and extended uncertainty is given according to specific demand.

3. SIMULATION SCHEME FOR IMAGE AND UNCERTAINTY

The level 1 product of the remote sensing measurement is the restored radiance data at the pupil plane through the radiation correction, which is also the general data available to the public users. For the infrared hyperspectral remote sensing process, the link of signal from the land surface emissivity (ε) and temperature (T) to the ground-leaving radiance (L_{GND}), the radiation at the top of atmosphere (L_{TOA}) the recoreding Digital Number data (DN), finally the restored radiance (L), includes the radiation coupling at ground, the atmospheric radiation transfer, the imaging of spectrometer, the radiation correction and other links, as shown in Figure 1.

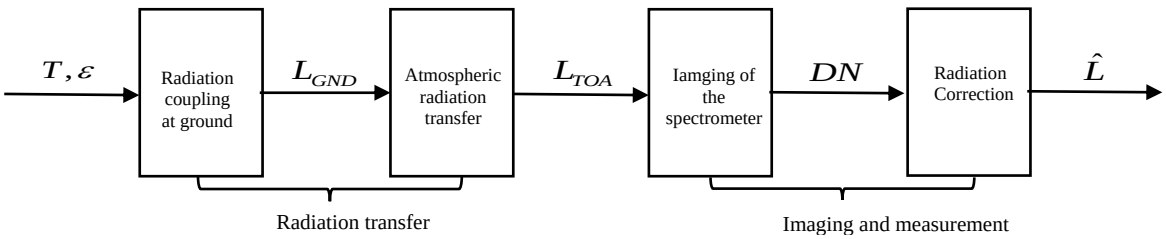

Figure 1. The forward transfer of remote sensing signals

The random signals of land surface temperature and emissivity are coupled and spread to the top of atmosphere and then become the restored radiance. Taking the restored radiance as the output of image chain simulation, the transfer process of radiation is sorted out to form the framework of the uncertainty tracing, and the key factors affecting the amplitude and uncertainty of infrared entrance pupil radiance spectral signal are shown in Figure 2.

The radiation coupling of surface temperature and emissivity spectra is converted into ground leaving radiance. Due to the influence of coupling radiation between the land surface and the atmosphere, the process radiation coupling includes surface reflection, surface emission and multiple reflection between the surface and the atmosphere. The uncertainty factors that can be traced to the surface radiation coupling process include the uncertainty of the land surface emissivity, the uncertainty of the land surface temperature, and the uncertainty of the terrain.

Then, the ground-leaving radiance is attenuated by the absorption and scattering effects of atmosphere and then reaches the sensor's pupil through atmosphere. Under the influence of adjacency effect and atmospheric path radiation, the radiation signal will increase. The uncertainty of atmospheric radiation is mainly affected by the variable components of the atmosphere. Therein, the influence of atmospheric trace gas is relatively fixed, Thus the influence of trace gas on the uncertainty of the inlet pupil signal can be ignored.

The imaging and measurement process is affected by the performance of the carrying platform, optical system and the detector. In this process, the signal is mixed with the system error and random noise of the instrument, making the data uncertain and the dimension of signal changed. During imaging and radiation correction process, the radiance signal is affected by the radiation, spatial, and spectral features of instrument. It is

firstly recorded as DN value data due to the influence of load radiation, space and spectral characteristics. The random errors of the imaging system such as the photon noise, the dark current noise, the background thermal noise and the system response nonlinearity add randomness to the DN value data. In the radiometric calibration process, random noise is also transferred to the superposition of the radiometric correction factor. After radiation correction, the DN value data is restored to radiance. The restored radiance is actually a measurement of the radiance of at the top of the atmosphere. There are also uncertainties from the radiometric calibration model, radiometric correction parameters and the DN data, which constitute the uncertainty in the measurement results of the radiance at the top of atmosphere.

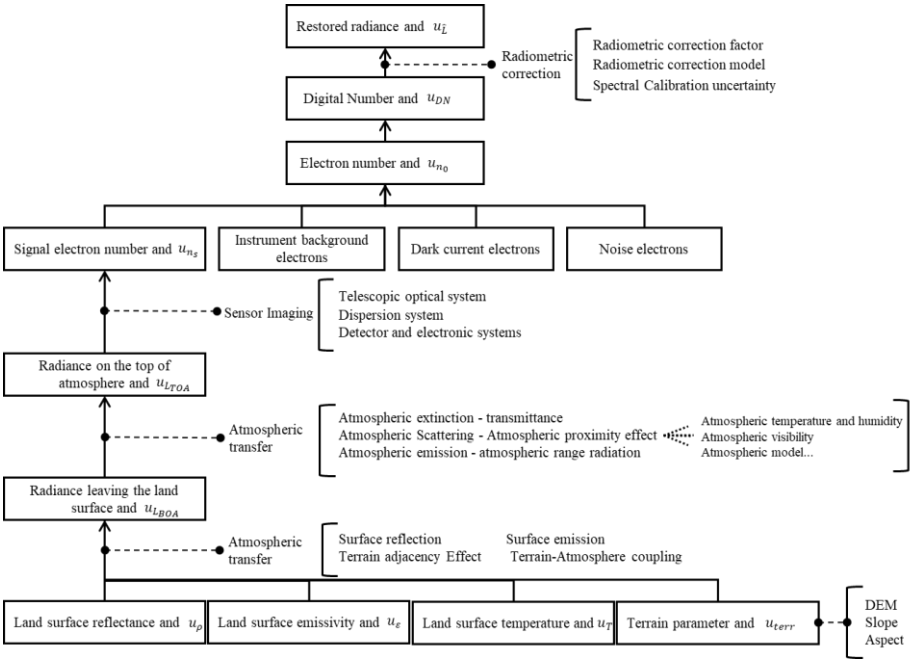

Figure 2. Simulation scheme for signal and uncertainty.

3.1 General Equations for Uncertainty Calculation

The uncertainty of primary components, such as the surface emissivity, the surface temperature, the Digital Elevation Map (DEM), the atmospheric temperature and humidity, as well as the instrument noise, should be considered in the uncertainty evaluation of the restored radiance, and gradually transferred upward. Firstly, the uncertainty is transferred to the radiance uncertainty at the top of atmosphere. Then, it is spread to the recording DN value. Finally, it is transferred to the restored radiance. Since the restored radiance is an indirect measurement object in the process of infrared hyperspectral remote sensing, its uncertainty needs to be synthesized for the contribution of each uncertainty component. The formula for calculating the synthesized uncertainty is as (1).

$$u_c = \sqrt{\sum_{i=1}^{m}\left(\left|\frac{\partial f}{\partial p_i}\right| u(p_i)\right)^2 + 2\sum_{1\le i\le j}^{m} r_{i,j}\frac{\partial f}{\partial p_i}u(p_i)\frac{\partial f}{\partial p_j}u(p_j)} \quad (1)$$

where, $u(p_i)$ is standard uncertainty of the directly measured p_i,

$\partial f / \partial p_i$ is the sensitivity of x_i in model f,

$r_{i,j}$ is the correlation coefficient between p_i and p_j,

m is the number of uncertainty components.

The uncertainty evaluation methods for direct measurement objects include type A and type B. In type A evaluation, the average of multiple independent repeated measurements is used as the best estimate, and the standard deviation calculated by Bessel formula is used as the standard uncertainty. According to the calibration certificate or manual and other sources, the method of type B assessment uses the multiple method, normal distribution method, uniform distribution method and other methods to determine the standard uncertainty of calculation by the probability distribution form.

If two measurement objects are calculated from the same measurement process or using related data sources, then the linear correlation coefficient need to be calculated with multiple sets of measurement or calculation data and used for uncertainty synthesis of indirect measurement objects. For the uncertainty transfer process of infrared hyperspectral remote sensing, there are many transfer links, so it is necessary to combine the two types of uncertainty evaluation methods of type A and type B. While the ground link, the atmosphere link, the imaging link are relatively independent, there are obvious correlation within the uncertainty contribution of different atmospheric elements, the different terrain parameters, the instrument parameters and radiation correction parameters, respectively.

3.2 Uncertainty from Ground to top of atmosphere (TOA)

According to our previous study on the radiative transfer model over rugged surface (Qiu, 2022), the radiance signal at the top of atmosphere could be divided into seven radiation components. Among them, five radiation components carry the information of target temperature and emissivity; one is the radiation from the adjacent pixel on land surface which scatters through the atmosphere and reaches the sensor. The last is the path radiation, which does not carry an effective signal from the surface. This paper constructs an uncertainty transfer chain from surface characteristics to the TOA radiance, as shown in Figure 3. The meaning of the parameters in Figure 3 is indicated in Appendix.

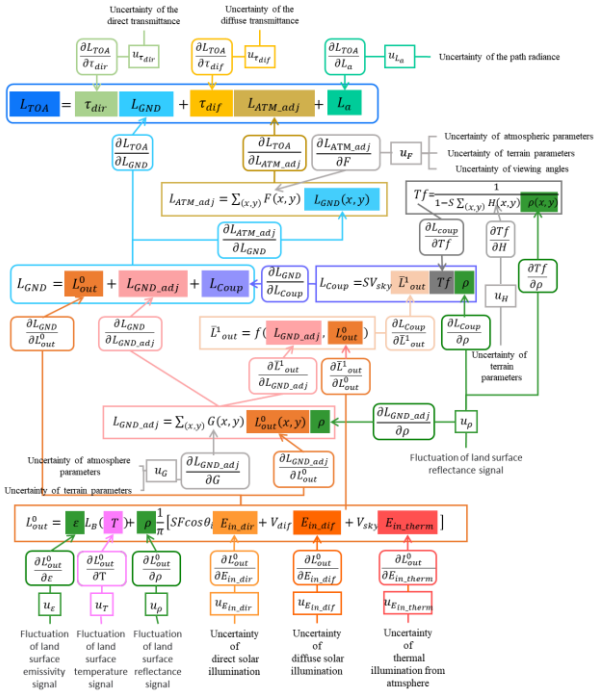

Figure 3. Uncertainty transfer chain from the ground to TOA

As shown in Figure 3, the uncertainty of the TOA radiance is derived from (1)atmospheric radiation components, such as direct atmospheric transmittance, the diffuse transmittance, the path radiation, the direct solar illumination, the solar scattering illumination, and the atmospheric thermal illumination; (2) topographic parameters, including the slope angle, the aspect angle, the sky visibility factor, the observation angle; (3) the fluctuations of surface characteristic signals such as surface emissivity, reflectivity, and temperature. These atmospheric parameters can be calculated from multiple output files of the MODTRAN radiative transfer model based on the established infrared radiated surface model. Therefore, the correlation coefficients between these atmospheric parameters need to be calculated. The calculation process of atmospheric parameters is complicated, but the factors affecting their uncertainty are same, including the uncertainty of the atmosphere radiation transfer models (such as MODTRAN) and the uncertainty of variable parameters of atmosphere. Therefore, the uncertainty evaluation method based on Monte Carlo is used to estimate the respective uncertainties and correlations of the six atmospheric parameters, in this paper. Under the given atmospheric conditions, random errors are assigned to total water vapor, total carbon dioxide, visibility and atmospheric temperature, and the uncertainty and correlation coefficient of corresponding output atmospheric parameters are calculated.

In this paper, the type B uncertainty evaluation method is used for the evaluation of MODTRAN model, and the empirical conclusions given in the MODTRAN User manual (Berk, 2008) are considered. The absolute error of transmittance is generally considered to be within ±0.005, and the relative error of radiation quantity is generally within ± 2%. Considering the 95% confidence probability under the normal distribution and the inclusion factor is set to 1.96, the standard uncertainty of transmittance caused by MODTRAN model is 0.003, and the standard relative uncertainty of radiation quantity is 1%.

3.3 Uncertainty for Imaging and Measurement Process

In this section, the traditional description methods of signal-to-noise ratio, noise equivalent temperature difference and radiometric calibration accuracy are not directly used. Instead, systematic random noise is superimposed in the dimension of electronic number signal, and the absolute uncertainty of calibration coefficient is used to quantify the radiometric correction error. The transmittance, diffraction efficiency, quantum efficiency, pixel size of detector and other parameters of the optical system are multiplication or division coefficients of the radiation signal transfer process. In the linear response range, these parameters determine the value of radiometric calibration gain coefficient. For the push-sweep imaging spectrometer, the point diffusion function of the imaging system has two dimensions: spatial and spectral dimensions. Assuming that the distributions of the point spread function in space and spectral dimensions are independent of each other, the point spread function could be described as a space-spectral function $PSF(x,y,\lambda)$. The uncertainty of TOA radiance accumulates in spectral and spatial dimensions, so that synthetic uncertainty of signal electrons could be analytically obtained, as shown in (2).

$$u_c(n_s)=\sqrt{\sum_{(x,y)}\sum_{\lambda}\left(\frac{\partial n_s}{\partial L_{TOA}(x,y,\lambda)}u_c\left(L_{TOA}(x,y,\lambda)\right)\right)^2} \quad (2)$$

$$\frac{\partial n_s}{\partial L_{TOA}}=\frac{\pi}{4}\frac{S}{F_{\#}^2}\frac{t_{\text{int}}}{hc}\lambda\tau_o(\lambda)\eta_d(\lambda)\eta_q(\lambda)SRF(\lambda)PSF(x,y,\lambda) \quad (3)$$

where, $SRF(\lambda)$ is the normalized spectral response function;

$PSF(x,y,\lambda)$ is the normalized point spread function;

λ is the wavelength;

x,y is the position of the target pixel.

The system shot noise, thermal background noise, dark current noise, quantization noise and readout noise are added to the electron number signal in the form of random errors. These noises would also remain in the recovered radiance spectrum after radiometric correction. The nonlinear response caused by the optical system, the nonuniform response rate of detector photosensitive element, the nonuniform response of amplifier array and the nonlinear error of readout circuit are all important reasons for nonuniformity of imaging system. The non-uniform and nonlinear response effects of the imaging system could be simplified as a multiplicative coefficient k_n in Figure 4. The meaning of the parameters in Figure 4 is indicated in Appendix.

The nonlinearity of the system δ describes the degree to which the output signal maintains a linear relationship with the input signal. It is a complex function of radiated power and is defined as the ratio of the maximum deviation between the actual response curve and the fitted line ($\Delta_{\max}$) with the difference between the maximum and minimum response $I_{\max}$ - $I_{\min}$ in linear interval, as shown in Equation (4). It is assumed that the nonlinear response coefficient follows Gaussian distribution. Thus, δ is 1.96 times of the uncertainty of nonlinear response coefficient (u_k), with the confidence probability of 95%.

$$\delta=\frac{\Delta_{\max}}{I_{\max}-I_{\min}} \quad (4)$$

Considering the random error caused by noise and response nonlinearity of the imaging system, the synthetic uncertainty of the DN recorded by detector could be expressed as equation (5).

$$u_c(DN)=\left|\frac{\partial DN}{\partial n_0}\right|u_c(n_0)=\frac{C_{VF}}{V_{REF}}\left(2^{bit}-1\right)u_c(n_0) \tag{5}$$

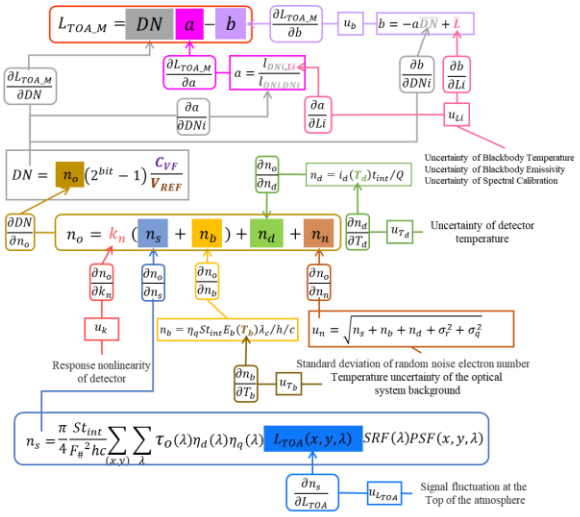

Figure 4. Uncertainty transfer chain from the TOA radiance to the restored radiance

Different levels of infrared radiation are usually generated using blackbodies at different temperatures, in laboratory calibration and on-orbit satellite calibration. Due to the random errors of blackbody and the temperature measurement, the sources of uncertainties of different levels of radiance ($u_c(L_i)$) include the uncertainty of the blackbody emissivity, the error of blackbody temperature, the non-uniformity of blackbody emissivity, and spectral calibration uncertainty.

In radiometric calibration process, the DN value needs to be obtained by repeated measurements. If there are M times of measurements, the uncertainty of the DN is times $1/\sqrt{M}$ comparing to uncertainty of a single measurement. Therefore, the contribution is small and the uncertainty of the calibration coefficient is mainly determined by $u_c(L_i)$. Under the condition of linear correction model, the variance and covariance of correction coefficients can be calculated according to the least squares, as shown in Equations (6) to (8). Then, σ_a and σ_b are uncertainties of calibration parameters, which could be used in the following uncertainty transfer.

$$\sigma_a^2=\frac{N\sum_{i=1}^{N}\left(L_i-\hat{a}DN_i+\hat{b}\right)^2}{(N-2)\left[N\sum_{i=1}^{N}DN^2{}_i-\left(\sum_{i=1}^{N}DN_i\right)^2\right]} \tag{6}$$

$$\sigma_b^2=\frac{\sum_{i=1}^{N}DN_i^2\sum_{i=1}^{N}\left(L_i-\hat{a}DN_i+\hat{b}\right)^2}{(N-2)\left[N\sum_{i=1}^{N}DN^2{}_i-\left(\sum_{i=1}^{N}DN_i\right)^2\right]} \tag{7}$$

$$\sigma_{ab}=\frac{\sum_{i=1}^{N}DN_i\sum_{i=1}^{N}\left(L_i-\hat{a}DN_i+\hat{b}\right)^2}{(N-2)\left[N\sum_{i=1}^{N}DN_i^2-\left(\sum_{i=1}^{N}DN_i\right)^2\right]} \tag{8}$$

According to the random error transfer formula, the uncertainty of DN value and the uncertainty of radiation correction coefficient were calculated, and the uncertainty of restored radiance was synthesized, as shown in (9).

$$u_c\left(L_{TOA\_M}\right)=\sqrt{\hat{a}^2u_c{}^2(DN)+DN^2\sigma_a{}^2+\sigma_b{}^2-2DN\sigma_{ab}} \tag{9}$$

where， r_{ab} is the correlation coefficient between the scaling gain coefficient and the bias coefficient; $\sigma_{ab}=r_{ab}\sigma_a\sigma_b$.

4. SIMULATION EXPERIMENTS

4.1 Validation of uncertainty model

In order to verify the uncertainty transfer model of the restored radiance, the parameters of an assumed geostationary satellite loading hyperspectral imager were used to simulate the image and uncertainty in the infrared band (3~12.5μm). The ground sampling interval of the medium-wave infrared channel and the long-wave infrared channel is 50 m and 100 m, respectively. The basic parameters of these two channels are shown in Table 1. Since the imaging data of medium wave and long wave infrared band are significantly affected by the shot noise jointly determined by dark current, thermal background irradiance, signal electron number and integration time, in order to improve the signal-to-noise ratio of the system, the hyperspectral imager adopts the method of multi-frame (20 frames) superposition to increase the number of repeated measurements for each pixel.

Instrument Parameter	Value	
	Mid-Wave Infrared	Long-Wave Infrared
Spectral domain (μm)	3.0~ 5.0	8.0~ 12.5
Spectral sampling interval (μm)	0.05	0.1
FWHM (μm)	0.040	0.079
Total MTF	0.17	0.17
Ground Sampling Distance (m)	50	100
Transmittance of optical system τ_{O1}	0.41	0.40
Spectrometer transmittance τ_{O2}	0.74	0.82
Diffraction efficiency η_d	0.89	0.89
Quantum efficiency η_q	0.65	0.45
$F_{\#}$	9.6	4.8
Detector pixel area S (m^2)	7.68×10^{-10}	7.68×10^{-10}
Integral Time(ms) t_{int}	20	0.3
Digitalizing bit bit	14	14
Output voltage V_{REF} (V)	3	3
Full well electrons e_{REF} (e^-)	3.00×10^6	1.125×10^7
System background temperature T_b (K)	100 K	100 K
Dark Current i_d (A/pixel)	1×10^{-12}	3×10^{-9}
Read out noise σ_r (e^-)	1600	4000
Quantizing noise σ_q	52.86	198.22
Response nonlinearity δ	0.5 %	0.5 %
Spectral scaling uncertainty	0.003 λ	0.003 λ
Relative uncertainty of blackbody emissivity u_{ε_R}	1 %	1 %
Relative uncertainty of blackbody temperature u_{Tc} (K)	0.1	0.1

Table 1. Instrument parameters for simulation experiment.

In this paper, the same rugged desert scene as in the previous simulation study of radiation transfer (Qiu, 2022) is used for

simulation experiments in this paper. The scene is located in the Mingsha Mountain in Dunhuang, Gansu Province, China. The types of ground objects in the experimental area mainly include cultivated land, buildings, desert and water bodies. Mingsha Mountains is a rugged and homogeneous desert area which is formed by the weathering and transport of the Gobi rocks in the northwest. The typical sunny slope and shady slope pixels are selected in the scene for uncertainty simulation, as shown in Figure 5. The imaging time corresponding to the simulation is set to July 14, 2019 at 6:38:45 (summer) and December 21, 2019 at 6:36:20 (winter).

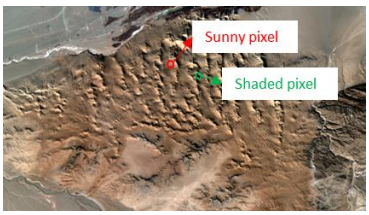

Figure 5. Scenario of simulation experiment.

The simulated dataset of TOA radiance spectrum contains random errors caused by topographic parameters, atmospheric parameters, land surface temperature and emissive uncertainty each. The spatial-spectral dimension convolution is performed on each TOA radiance spectrum, while the random noise and nonlinear response error are added to the DN spectrum. Then, when each DN value spectrum was radiometric corrected to obtain the restored radiance spectrum. Totally 625 random spectra of each pixel were obtained, taking into account the uncertainties of the imaging link and the radiometric correction link. The verification of the uncertainty of the restored radiance is shown in Figure 6. For each pixel and each band, more than 99.9% of the simulated radiance spectra are within the range of $\pm 3\ \sigma$ determined by the analytical model. Meanwhile, the distribution range of the simulated radiance of random experiments is in good agreement with the range of $\pm 3\ \sigma$ determined by the uncertainty.

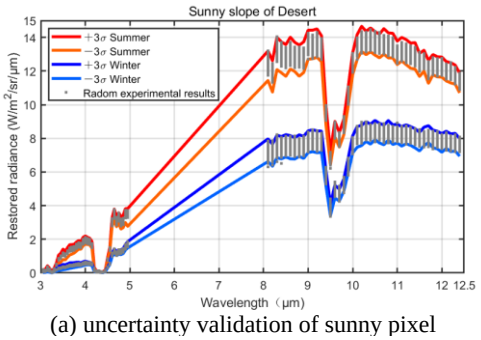

(a) uncertainty validation of sunny pixel

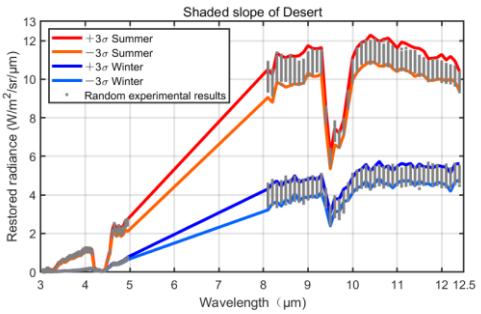

(b) uncertainty validation of shaded pixel

Figure 6. Validation of uncertainty model.

4.2 Ranking of the uncertainty contributors

The calculated restored radiance uncertainty includes the surface uncertainty component, the atmospheric parameter uncertainty component, the topographic parameter uncertainty component, and the imaging and calibration process uncertainty component, as shown in (10).

$$\frac{u_c\left(L_{TOA\_M}\right)}{L_{TOA\_M}} = \sqrt{\left(u_{GND}\right)^2 + \left(u_{ATMO}\right)^2 + \left(u_{TERR}\right)^2 - \left(u_{I\&C}\right)^2} \quad (10)$$

where, u_{GND}, u_{ATMO}, u_{TERR} and $u_{I\&C}$ are the relative uncertainty of recovered radiance introduced by ground signals, atmospheric parameters, topographic parameters, imaging and calibration link, respectively.

By controlling variables, the standard uncertainty calculation of restored radiance under the influence of single uncertainty factor is designed respectively. It can be seen from the Figure 6, that the uncertainty of the restored radiance of the shaded slope pixels is relatively large in winter. In this paper, the simulated data of winter shady slope pixels are used to rank the uncertainty factors. The relative uncertainty of shady pixel in winter synthesized by each link is obtained, as shown in Figure 7(a). In winter, the temperature of the desert shady slope is very low, and the received solar and downward illumination is less. Therefore, the corresponding signal level of this pixel is low, and the uncertainty caused by it increases. It could be obtained that the order of uncertainty factors on the restored radiance is, from large to small, the uncertainty of imaging and calibration, the fluctuation of surface signal, the uncertainty of terrain parameters, and the uncertainty of atmospheric parameters.

Further analysis of the restored radiance formula in (9) shows that the uncertainty of the restored radiance consists of four components: $a^2 u_c^{\ 2}(DN)$, $DN^2 u_c^{\ 2}(a)$, $u_c^{\ 2}(b)$ and $2DN\sigma_{ab}$. Their contribution on the uncertainty of the recovered radiance is shown in Figure 7(b). It is obvious that the DN uncertainty of including instrument noise and nonlinear error noise has the greatest influence on recovered radiance. While the contribution of the covariance σ_{ab} of the sum of the correction coefficients is the second important factor.

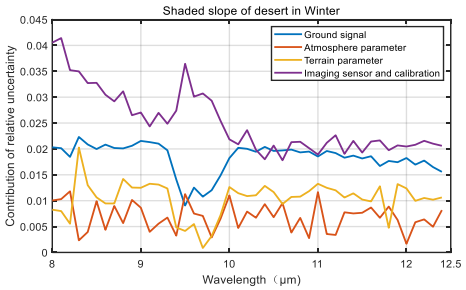

(a) Ranking of uncertainty contributions.

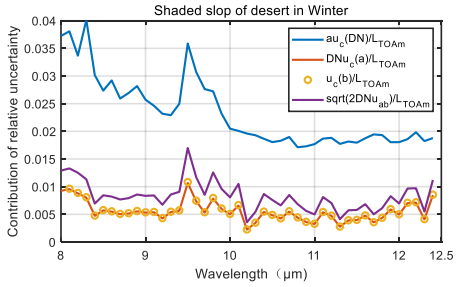

(b) Ranking of uncertainty contributions of imaging and correction link.

Figure 7. Ranking of uncertainty contributions of different links.

5. CONCLUSIONS

The traditional end-to-end image chain simulation tools do not describe the uncertainty synthesis process quantitatively. In this paper, a new image chain simulation scheme was established to modeling the hyperspectral imaging uncertainty. In the forward model of remote sensing, the uncertainty contributions derived from the fluctuations of surface temperature and the land surface emissivity, atmosphere, terrain, imaging systems, and calibration processes were compounded. Then the uncertainty model was applied to practice, and the influence of uncertainty sources were compared and ranked. The validity of the uncertainty transfer model was conducted by using the restored radiance obtained in randomized simulation experiments. More than 99.9% of the stochastic simulation radiance spectra are in the range of triple standard uncertainty predicted by our model for both sunny slope and shady slope of desert. Under the simulation condition of this paper, the uncertainty introduced by the system noise and the covariance of the radiation correction coefficient are the leading uncertainty contributor, which can provide reference for the error allocation and design optimization of the remote sensing process of the system. We hope that the uncertainty model proposed in this paper, could provide reliable reference to the development of spaceborne hyperspectral imaging systems and the application systems.

REFERENCES

Tang H., Li Z. Quantitative Remote Sensing in Thermal Infrared. Berlin, Heidelberg: Springer Berlin Heidelberg, 2014: 203-247.

Johnson W.R., Hook S.J., Mouroulis P., et al. HyTES: Thermal imaging spectrometer development. 2011 Aerospace Conference. Big Sky, USA: IEEE, 2011: 1-8. DOI: 10.1109/AERO.2011.5747394.

Yuan L., Xie J., He Z., et al. Optical design and evaluation of airborne prism-grating imaging spectrometer. Optics express, 2019, 27(13): 17686-17700. DOI: 10.1364/OE.27.017686.

Schott J.R. Remote Sensing: The Image Chain Approach. 2nd ed. New York: Oxford University Press, 2007: 17-21.

Goodenough A.A., Brown S.D. DIRSIG5: Next-Generation Remote Sensing Data and Image Simulation Framework. IEEE Journal of Selected Topics in Applied Earth Observations and Remote Sensing, 2017, 10(11). DOI: 4818-4833.10.1109/JST ARS.2017.2758964

Cota S.A., Lomheim T.S., Florio C.J., et al. PICASSO: an end-to-end image simulation tool for space and airborne imaging systems II. Extension to the thermal infrared: equations and methods. Imaging Spectrometry XVI. San Diego, California, USA: SPIE, 2011: 81580G. DOI: 10.1117/12.892808.

Segl K., Guanter L., Rogass C., et al. EeteS—The EnMAP End-to-End Simulation Tool. IEEE Journal of Selected Topics in Applied Earth Observations and Remote Sensing, 2012, 5(2): 522-530. DOI:doi: 10.1109/JSTARS.2012.2188994.

Qiu, X.; Zhao, H.; Jia, G.; Li, J. Atmosphere and Terrain Coupling Simulation Framework for High-Resolution Visible-Thermal Spectral Imaging over Heterogeneous Land Surface. Remote Sens. 2022, 14, 2043. DOI: https://doi.org/10.3390/rs14092043

BIPM, IEC, IFCC, ILAC, ISO, IUPAC, IUPAP, and OIML. Evaluation of measurement data — Guide to the expression of uncertainty in measurement. Joint Committee for Guides in Metrology, JCGM 100:2008. URL: https://www.bipm.org/documents/20126/2071204/JCGM_100_2008_E.pdf/cb0ef43f-baa5-11cf-3f85-4dcd86f77bd6

Man, Y.; Reasearch progress of on-board absolute radiometric calibration for optical remote sensing satellite. Chinese Space Science and Technology, 2022, 42(6):12-22 (in Chinese).

Berk A., Anderson G.P., Acharya P.K. MODTRAN 5.3.2 USER'S MANUAL. Spectral Sciences Inc, 2008.

APPENDIX

In this section the meaning of parameters using in the Figure 3 and 4 are explained, as following.

μ_* denotes the uncertainty of the variable *;

L_{TOA} is the radiance at the top of the atmosphere;

τ_{dir} represents the direct atmospheric transmittance;

τ_{dif} represents the atmospheric scattering transmittance;

L_{ATM_adj} is the radiance of atmospheric adjacency effect;

L_{GND_adj} is the radiance of terrain adjacency effect;

θ_i is the angle of incidence of the sun;

V_{dif} is the proportion of scattered solar radiation received by the slope relative to the horizontal plane;

E_{in_dir} is the direct solar irradiance;

E_{in_dif} is the irradiance diffused by the sky;

E_{in_therm} is the downward thermal irradiance of atmosphere;

L_a is the atmospheric path radiance;

F is the atmospheric adjacency effect contribution function;

H is the contribution function of atmosphere-terrain coupling;

G is contribution function of terrain adjacency illumination;

V_{sky} is the sky visibility factor;

L_{coup} is the coupled radiance;

a is the gain coefficient of the radiometric correction;

b is the bias coefficient of the radiometric correction;

L_{TOA_M} is the recovered radiance;

n_0 is the total number of electrons received by the detector;

bit represents quantization bits;

C_{VF} is the gain factor;

V_{REF} is the reference voltage of readout circuit;

n_s is the number of signal electrons;

n_b is the number of background thermal noise electrons;

n_d is the number of dark current electrons;

n_n is the number of random noise equivalent electrons;

k_n is the random responsivity caused by nonlinearity of detector;

h is the Planck's constant;

c is the speed of light.